Anisotropic magnetization, critical temperature, and paramagnetic Curie temperature in the highly anisotropic magnetic Heusler compound Rh_2CoSb

Yangkun He,[1,*] Romain Sibille,[2] Dong Chen,[1] Johannes Kroder,[1] Toni Helm,[1,3] Walter Schnelle,[1] Claudia Felser,[1] and Gerhard H. Fecher[1]

[1]*Max-Planck-Institute for Chemical Physics of Solids, D-01187 Dresden, Germany*

[2]*Laboratory for Neutron Scattering and Imaging, Paul Scherrer Institut, 5232 Villigen PSI, Switzerland*

[3]*Dresden High Magnetic Field Laboratory (HLD-EMFL), Helmholtz-Zentrum Dresden–Rossendorf, 01328 Dresden, Germany*

(Received 6 April 2021; revised 18 May 2021; accepted 4 June 2021; published 21 June 2021)

The paramagnetic Curie temperature θ_p is a concept that describes the magnetic ordering temperature in the well-established Curie-Weiss law. Despite the successful explanations of the magnetic behavior, the anisotropy is not usually considered. Although anisotropic θ_p has been reported for several layered antiferromagnetic or ferrimagnetic materials owing to the orientation-dependent exchange, in ferromagnetic systems, θ_p was thought to be almost isotropic for decades, and the occasionally reported small difference has remained unexplained. In this paper, we experimentally report the anisotropic magnetization, critical temperature, and paramagnetic Curie temperature in highly anisotropic magnetic Rh_2CoSb caused by a large magnetocrystalline anisotropy. The saturation magnetization along the c axis is 25% larger than that along the a axis. The critical temperature and paramagnetic Curie temperature along the c axis are 6 and 15 K higher than those along the a axis, respectively, as deduced from the Arrott plots and inverse susceptibility. A simple modification of the Curie-Weiss law was made to calculate the anisotropic θ_p, which well explains not only Rh_2CoSb, but also many other previously reported ferromagnetic materials.

DOI: 10.1103/PhysRevB.103.214436

I. INTRODUCTION

The magnetocrystalline anisotropy K_1 is the energy that forces the moments to align along the easy axis. Various phenomena related to this energy in magnetism, such as magnetostriction [1], hard magnetism [2], and anisotropic magnetoresistance [3], have been studied and applied in our daily lives. However, there are also several less well-known effects related to K_1, including anisotropic magnetization [4,5], critical temperature, and paramagnetic Curie temperature [6,7].

The magnetization along the easy axis is larger than that along the hard axis because, under the effect of both thermal energy and K_1, the moments lie in a narrow cone along the easy axis, whereas a wider cone appears for magnetization along the hard axis [4]. The difference in magnetization along both axes is negligible in ordinary $3d$ ferromagnets. For example, the ratios of anisotropic magnetization or saturation magnetization (anisotropic magnetization ratio $\Delta m/m$) are $\sim$0.01% for Fe and Ni [8]. However, in highly anisotropic systems, the values are much larger: 4% for YCo_5 [9,10], 5% for MnBi [11,12], and 9% for Fe_2P [13].

A ferromagnet loses its spontaneous long-range-ordered moment at the Curie temperature, above which thermal energy overcomes the magnetic interactions, leading to paramagnetism. However, the concept of Curie temperature is only valid along the easy axis in whose direction the moments spontaneously align at the zero field. Applying a magnetic field enables the moments to be forcibly aligned away from the easy axis or even along the hard axis with the magnetic ordering below a critical temperature (T_c). Generally, for most magnetic materials, the critical temperature is similar to the Curie temperature. However, being "similar" is not equivalent to being the "same." Callen reported in a theoretical work that a large K_1 and a small exchange energy can lead to an anisotropic critical temperature [6]. Thereafter, ferrimagnetic Fe_7S_8 was reported to be paramagnetic along the c axis and ferromagnetic on the ab plane [7], in agreement with the theoretical prediction. However, little evidence has been found in most ferromagnetic systems.

The paramagnetic Curie temperature θ_p is another concept for describing the magnetic ordering temperature by fitting the inverse susceptibility in the paramagnetic state using the Curie-Weiss law, which is usually higher than the Curie temperature. Above θ_p, the short-range-ordered magnetic structures vanish. Despite the successful explanation of the magnetic behavior, the anisotropy is not considered in the Curie-Weiss law. However, it was found that, in several layered antiferromagnets (e.g., $TbRh_2Si_2$ [14]) and ferrimagnets (e.g., Fe_7S_8 [7]), θ_p can be significantly different between the

*yangkun.he@cpfs.mpg.de

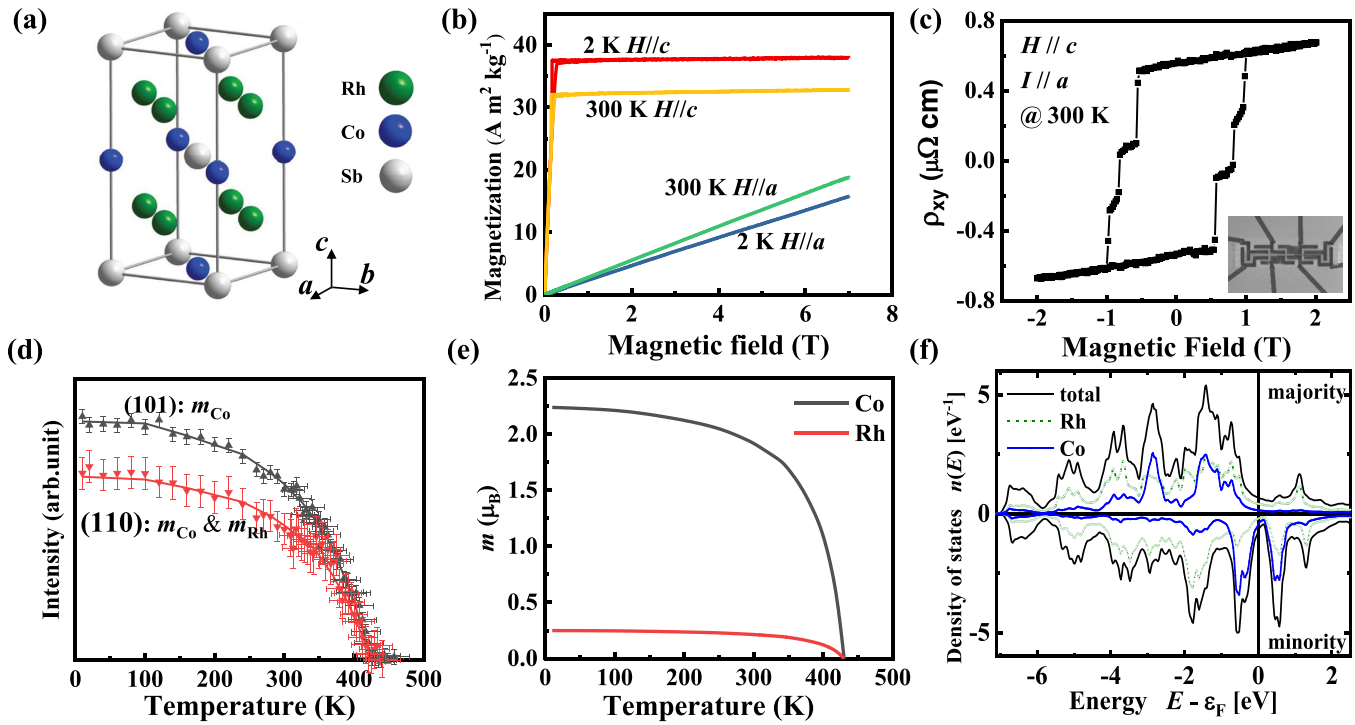

FIG. 1. Hard magnetic properties of Rh_2CoSb. (a) Crystal structure. (b) Magnetization curves along the c and a axes at 2 and 300 K. (c) Hall resistivity of a single crystal cut by a focused iron beam (FIB) with a width of 1.37 μm and a thickness of 1.16 μm. The inset shows the image of the FIB sample. The large coercivity of approximately 1 T determined from the anomalous Hall effect (c) is indicative for the large K_1. (d) Intensities of the (101) and (110) peaks of the neutron diffraction. The intensity of the (101) peak is only related to the Co moment, whereas the intensity of the (110) peak is related to both the Co and the Rh moments. The solid curves are the intensities for both magnetic Bragg reflections calculated to provide good agreement with the overall temperature dependence and assuming that both the Co and the Rh moments follow the same order parameter. (e) Temperature dependence of the magnetic moment value. (f) Calculated density of states. Rh is spin polarized.

hard and easy axes even with different signs. This is explained by the ferromagnetic in-plane exchange interaction and antiferromagnetic coupling between the layers along the c axis.

Compared with antiferromagnetic systems where anisotropic exchange interactions play a decisive role in θ_p, ferromagnetic systems usually have ferromagnetic interactions in all directions. Therefore, θ_p was thought to be almost isotropic for decades and the occasionally reported small difference has remained unexplained [15,16]. In theory [6,17,18], a large anisotropic θ_p in ferromagnetic materials can also be realized in systems with a large crystal field, although only a few reports exist.

Rh_2CoSb is a tetragonal Heusler crystallized in the $D0_{22}$ structure with $a = 4.0393(6)$ and $c = 7.1052(7)$ Å. The $4d$ $(0\ \frac{1}{2}\ \frac{1}{4})$ site is occupied by Rh, $2b$ $(0\,0\,\frac{1}{2})$ by Co, and $2a$ (0 0 0) by Sb as shown in Fig. 1(a). Rh_2CoSb is a hard magnet with a K_1 of 3.6 MJ m^{-3} and a Curie temperature of around 450 K [19]. The anisotropy field is 17.5 T at 2 K and 12 T at 300 K obtained from extrapolation as shown in Fig. 1(b). The magnetic hardness parameter is $\kappa = 4.1$ at 2 K and 3.7 at 300 K, which is the largest among all rare-earth free magnets that exhibit saturation magnetization $\mu_0 M_s > 0.4$ T. The highly anisotropic magnetic properties of Rh_2CoSb provide a good opportunity to study the anisotropic magnetization, critical temperature, and paramagnetic Curie temperature in this system.

In this paper, we report the anisotropic magnetization, critical temperature, and paramagnetic Curie temperature in single crystals of ferromagnetic Rh_2CoSb. A large anisotropic magnetization ratio of 25% is observed. The anisotropic critical temperature and paramagnetic Curie temperature are dominated by the crystal field, which can be estimated using magnetocrystalline anisotropy.

II. EXPERIMENTAL DETAILS

Single crystals were grown using the Bridgeman method [19]. The composition of the crystals was determined by

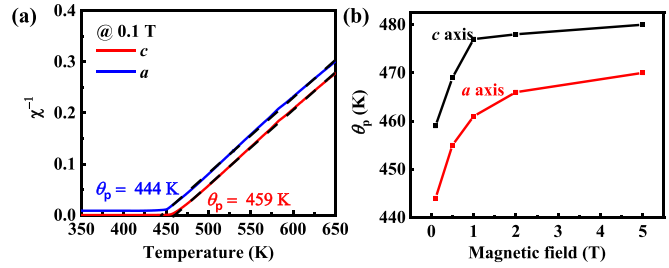

FIG. 2. (a) Temperature dependence of inverse susceptibility along both the c and the a axes. (b) Magnetic-field dependence of θ_p along the c and a axes.

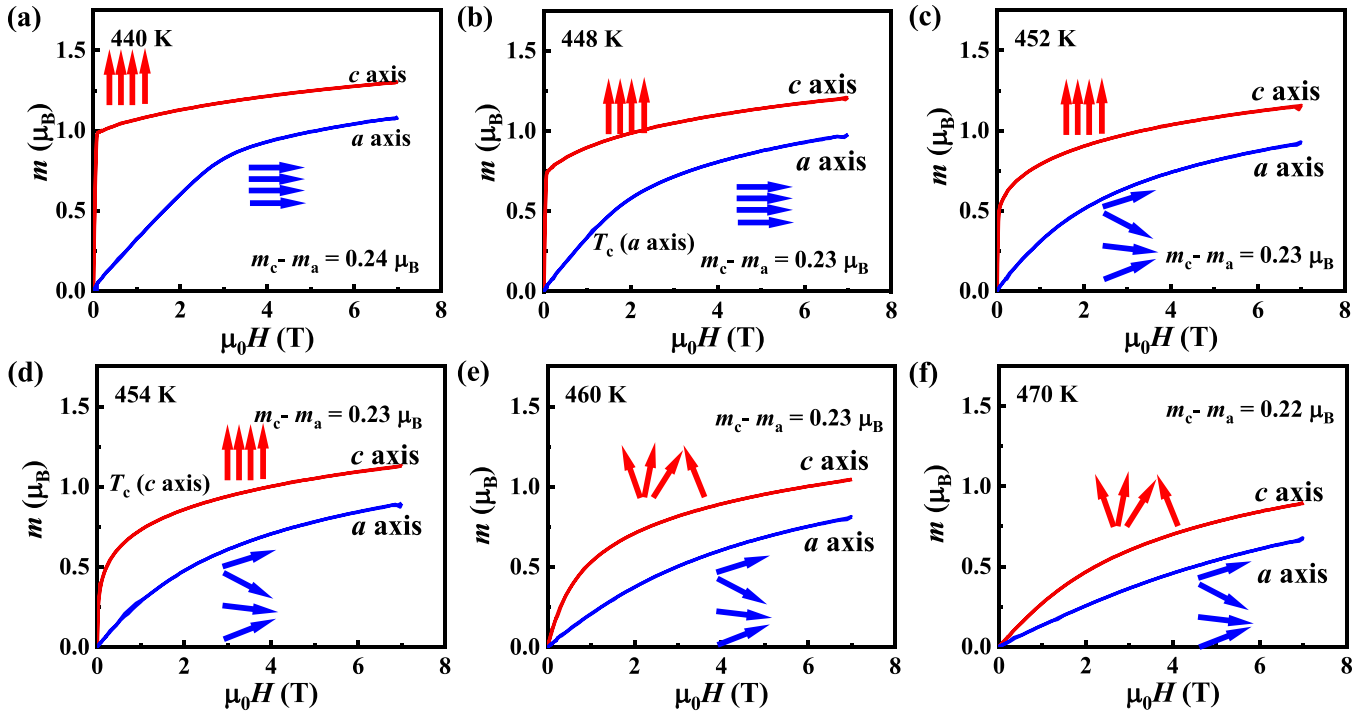

FIG. 3. Magnetization curves along the c and a axes around the Curie temperature. The inserted (non)parallel arrows schematically sketch the long-range (dis)ordered magnetic structure.

wavelength dispersive x-ray spectroscopy, which showed a homogenous composition of $Rh_{50.3}Co_{25.6}Sb_{24.1}$. The magnetization was measured on single crystals with a magnetic field applied along either the a or the c axis using a vibrating sample magnetometer (magnetic property measurement system 3, Quantum Design). The sample size was $0.65 \times 0.78 \times 1.30\,\mathrm{mm}^3$. Single-crystal neutron diffraction was performed on the Zebra instrument at the Swiss Spallation Neutron Source SINQ of the Paul Scherrer Institute in Villigen, Switzerland. The instrument was operated in four-circle geometry using an Eulerian cradle, and the energy of the incoming beam was selected using a Ge(311) monochromator, resulting in a wavelength of approximately 1.175 Å. To cover the entire temperature range, we conducted two experiments on the same sample using a close-cycle refrigerator between 10 and 320 K and a vacuum furnace operated between 300 and 480 K. About 120 Bragg reflections were measured at fixed temperatures of 10, 300, and 480 K. The integrated intensities were analyzed using the FULLPROF software suite [20] to refine the nuclear and magnetic structures.

III. RESULTS

As Rh_2CoSb is a highly anisotropic material, its coercivity can easily reach 1 T when the crystal dimension is decreased to 1.37 μm as can be seen in the anomalous Hall effect measurements in Fig. 1(c). The total moment of $2.6\mu_B$ per formula unit is contributed by ferromagnetically coupled Co and Rh. This was confirmed by our neutron-diffraction study, which obtained ordered moments of $0.25 \pm 0.06\,\mu_B$ and $2.24 \pm 0.05\mu_B$ at 10 K for Rh and Co, respectively. Their temperature dependence was studied by following the intensity of two magnetic Bragg reflections as shown in Fig. 1(d). The reflections were selected to attempt to distinguish the evolution of the two moments. Although the data over the entire temperature range can be accounted for by assuming that Rh and Co follow the same order parameter [Figs. 1(d) and 1(e)], significant deviations from this idealized behavior cannot be excluded from the statistics of the present experiment. In particular, our calculation [21] in Fig. 1(f) shows that the Co moment is more localized and that the Rh moment is induced as also inferred from the unquenched Co orbital moment from our previous x-ray magnetic circular dichroism experiment [19]. In this scenario, the coupling between Rh and Co could decrease drastically upon approaching the Curie temperature and as a result Rh loses its magnetism quickly, which causes the abnormal behavior in the AC susceptibility in addition to the Hopkinson effect [19,22].

We checked the paramagnetic Curie temperatures based on the inverse susceptibility in Fig. 2. For this, we fit temperature-dependent data along both axes using the Curie-Weiss law,

$$\chi = C/(T - \theta_p), \tag{1}$$

where χ is the susceptibility and C is the Curie constant. When the applied magnetic field is 0.1 T, the values of θ_p along the c and a axes are 459 ± 1 and 444 ± 1 K, respectively, as shown in Fig. 2(a). The Curie constants for both axes are the same, corresponding to an effective moment of $1.96\,\mu_B$, which roughly agrees with the measured ordered moment of $2.6\mu_B$ at 2 K. Figure 2(b) shows the θ_p calculated from the data measured with different magnetic fields. Notably, θ_p along both axes exhibits a field dependence, which

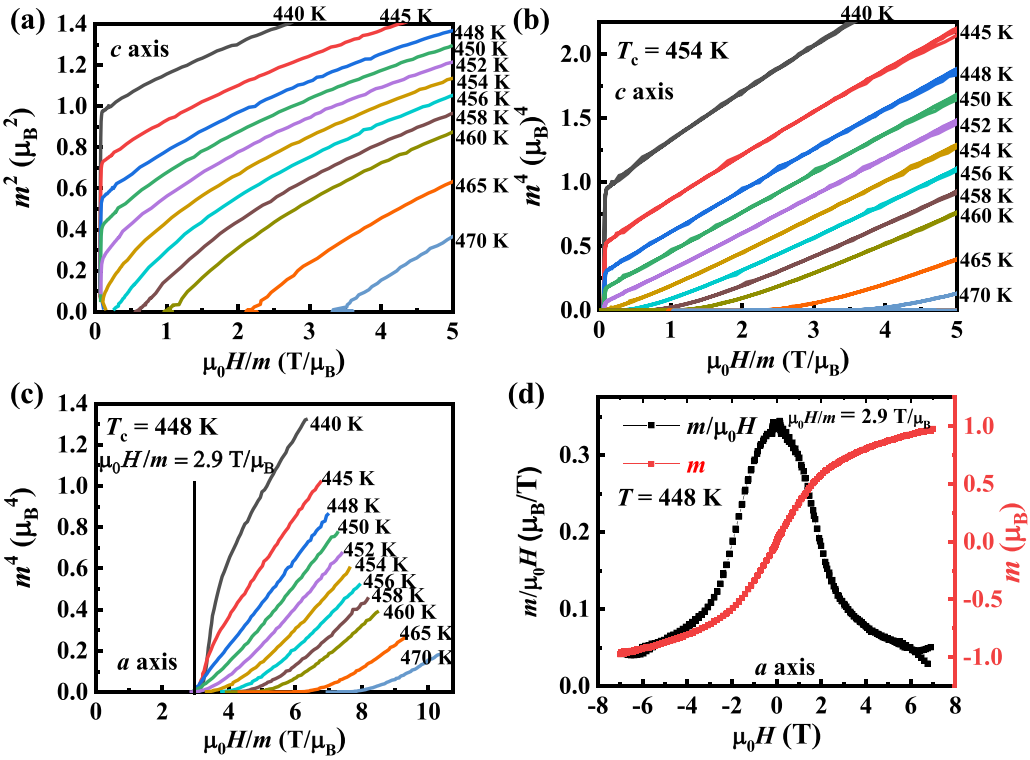

FIG. 4. (a) Arrott curves of M^2 vs H/M along the c axis. Modified Arrott curves of M^4 vs H/M along the (b) c and (c) a axes. (d) Susceptibility and magnetization when H was along the a axis at 448 K.

can be explained by the field-dependent susceptibility due to the short-range order when the temperature is not too far from the Curie temperature. Even in the paramagnetic region, the magnetization curve is not linear, and the susceptibility χ decreases with increasing field. As a result, θ_p increases with increasing magnetic field. However, the difference between the c and the a axes does not change and the value is always between 12 and 15 K.

The magnetization curves close to the Curie temperature along both the c and the a axes are shown in Fig. 3. The magnetization along the c axis is significantly larger than that along the a axis. The difference is 0.24 μ_B per formula at 440 K and 7 T, which is about 25% of the total moment, a value that is much larger than that in YCo_5 (4% at 4.2 to 300 K under 20 T [9,10]), MnBi (5% at 5 K under 6 T [11,12]), and Fe_2P (9% at 5 K under 7 T [13]). The anisotropic crystal fields together with the large spin-orbit coupling, are responsible for highly anisotropic magnetization. The difference in magnetization along the c and a axes decreases with increasing temperature, although it still exists in the paramagnetic state as shown in Fig. 3(f). The first impression on critical temperatures can be obtained by the bare eye when considering the $M(H)$ magnetization curves at different temperatures. Below 454 K, the magnetization curves along the c axis saturate (in a single-domain state) rapidly as shown in Figs. 3(a)–3(d). At higher temperatures [Figs. 3(e) and 3(f)], the initial susceptibility decreased and the magnetization was a bent curve. Therefore, the critical temperature for the c axis (also the Curie temperature) was around 454 K. The magnetization curve along the a axis is linear before saturation at 440 K, and it saturates at approximately 3.2 T. However, above 452 K, the curve is no longer linear at low field, indicating that the critical temperature along the a axis is lower than 452 K.

The Arrott curves of M^2 vs H/M were used to precisely determine the critical temperature T_c for H along the c axis as shown in Fig. 4(a). In theory, the high-field curves should be a series of parallel straight lines in the high-field range, and the intercept of M^2 is positive below T_c and negative above T_c. However, all the curves in this plot are nonlinear with a downward curvature even in the high-field region, which indicates that the long-range Landau mean-field theory is not satisfied for Rh_2CoSb. Instead, a tricritical mean-field model (M^4 vs H/M) [23,24] is used, and a good fit is obtained as shown in Fig. 4(b). In this model, where the critical exponents β, γ, and σ are 0.25, 1, and 5, respectively, the magnetic phase transition is three dimensional, indicating a nearly isotropic exchange interaction. The T_c of the c axis was determined to be 454 $\pm$ 1 K.

Similarly, a tricritical mean-field model was also used to determine T_c for the a axis as shown in Fig. 4(c). The a axis is the hard axis, and the initial susceptibility χ_0 is only 0.35 μ_B T^{-1} [Fig. 4(d)], which is far smaller than that along the c axis. Therefore, the intercept on χ_0^{-1} (2.9 Tμ_B^{-1}) was used to determine T_c rather than zero along the c axis. This method is also used in polycrystalline samples, whose χ_0^{-1} values are also far from zero [25]. The modified Arrott curves (M^4 vs H/M) showed a T_c of 448 $\pm$ 1 K. This value is 6 K below that for the c axis, which is not due to the inaccuracy of the measurement.

IV. DISCUSSION

According to a previous theory [17,18], the values of θ_p along the c and a axes (i.e., θ_p^c and θ_p^a, respectively) are determined by both the exchange and the crystal field as follows:

$$\theta_p^c = -\frac{J(J+1)}{3k_B}J_{ex}^c - \frac{(2J-1)(2J+3)}{5k_B}B_2^0, \quad (2)$$

$$\theta_p^a = -\frac{J(J+1)}{3k_B}J_{ex}^a + \frac{(2J-1)(2J+3)}{10k_B}B_2^0, \quad (3)$$

where B_2^0 is a crystal-field parameter; J is the total angular moment of the atom; J_{ex}^c and J_{ex}^a are the sum over all exchange constants along the c and a axes, respectively; and k_B is the Boltzmann constant. The first term is related to the exchange, whereas the second term is related to the crystal field. These two equations have already been proven to work in antiferromagnetic systems [14,26] dominated by the anisotropic exchange. In Rh_2CoSb, assuming that $J_{ex}^c \approx J_{ex}^a$ for a ferromagnetic interaction (from the tricritical mean-field model in Fig. 4), we can deduce the theoretical difference in θ_p between the c and a axes $\Delta\theta_p$ from

$$\Delta\theta_p = \theta_p^c - \theta_p^a = -\frac{3(2J-1)(2J+3)}{10k_B}B_2^0. \quad (4)$$

Assuming $J \approx 1$ from the effective moment determined from the inverse susceptibility, one can calculate B_2^0/k_B using Eq. (4) as -10 K and $J_{ex}^c/k_B \approx J_{ex}^a/k_B = -674$ K. Here, a negative sign belongs to a ferromagnetic interaction. In first approximation the B_2^0 (usually B_2^0 is written with the symbol D) is related to K_1 by the relation $K_1 = B_2^0 J^2/V$, where V is the volume per magnetic atom. Because Rh only provides a small induced spin moment without anisotropy, whereas Co provides both spin and orbital moments related to magnetocrystalline anisotropy, V is roughly equal to the volume of the primitive cell. K_1 is estimated as 2.4 MJ m^{-3} from the above relation, which roughly agrees with the experimental value of 3.6 MJ m^{-3}.

Since the crystal field is difficult to measure and, usually, B_2^0 is unknown, it is difficult to predict $\Delta\theta_p$. However, below the Curie temperature, the crystal field will lead to magnetocrystalline anisotropy in ferromagnetic materials and, thus, we can roughly estimate $\Delta\theta_p$ in the following way, assuming an isotropic exchange in ferromagnetic systems:

$$\Delta\theta_p = K_1 V/k_B. \quad (5)$$

Here, positive values of K_1 and $\Delta\theta_p$ indicate the easy axis and a higher temperature along the c axis, respectively. In Rh_2CoSb, the K_1 of 3.6 MJ m^{-3} is relatively large for a rare-earth free magnet. We obtained $\Delta\theta_p = 15$ K from Eq. (5), which is exactly equal to the measured value, further confirming that the crystal field is the origin of all the above phenomena rather than the anisotropic exchange. We compared our theory with previous reports on some ferromagnetic materials in Fig. 5 and found that it works quite well. The slope of the curve is close to the Boltzmann constant k_B.

The magnetocrystalline anisotropy varies from 10^0 to 10^4 kJ m^{-3} in ferromagnetic materials. Therefore, $\Delta\theta_p$ calculated using Eq. (5) varies from 10^{-3} to 10^1 K. Assuming an isotropic exchange, J_{ex}, we can modify Eqs. (2) and (3) as

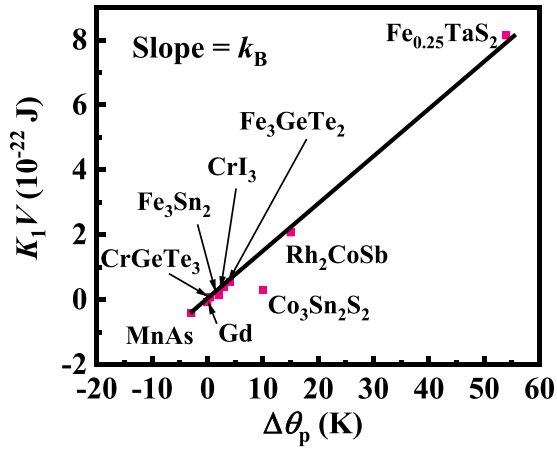

FIG. 5. Relationship between K_1V and $\Delta\theta_p$ for some ferromagnetic materials. References can be found in Table I.

$$\theta_p^c = -\frac{J(J+1)}{3k_B}J_{ex} + \frac{2}{3}K_1V/k_B, \quad (6)$$

$$\theta_p^a = -\frac{J(J+1)}{3k_B}J_{ex} - \frac{1}{3}K_1V/k_B. \quad (7)$$

From Eq. (7), there is a possibility that, for ferromagnets with an extremely large K_1 and a small exchange constant (low Curie temperature), θ_p along the hard axis could even be negative, in contrast to the ferromagnetism. This has also been reported for some U-based compounds, such as U_2RhSi_3 [27], UPtAl [28], UIr [29], or $UCo_{0.5}Sb_2$ [30]. In these compounds, the anisotropy plays an even more important role than the exchange on θ_p along the hard axis.

The calculated $\Delta\theta_p$ works well for most ferromagnetic materials as shown in Table I. However, for antiferromagnetic/ferrimagnetic materials and magnetic materials with complicated spin structures, Eq. (5) is only valid for the sign of $\Delta\theta_p$, indicating that the anisotropic exchange is dominant. In these cases, $\Delta\theta_p$ can be as large as 100 K, which is an order larger than the effect of the crystal field. This is one reason why previous reports on anisotropic $\Delta\theta_p$ mainly focused on antiferromagnetic and ferrimagnetic materials.

Recently, an anomalous increase in the Curie temperature along the c axis in ferromagnetic $CrTe_2$ with decreasing thickness has been reported [43]. This is explained as the change from the easy-plane to the easy-axis spin structure, which further supports our theory that anisotropy plays an important role in the magnetic ordering temperature.

Of the anisotropic magnetic properties, magnetization is the easiest parameter to obtain. Therefore, compared with antiferromagnetic or ferrimagnetic materials whose magnetization is small, ferromagnetic materials show a much larger magnetization, whose signal can be detected and used in sensors for temperature measurement. Besides the temperature, the anisotropic critical temperature can also be used to detect the orientation. The difference in magnetization can be clearly observed close to or even above the Curie temperature. The ferromagnetic ordering can be turned on and off by changing

TABLE I. Comparison of the anisotropic magnetization $\Delta m/m$ and paramagnetic Curie temperature $\Delta\theta_p$ in different materials.

Materials	Category	K_1 (MJ m^{-3})	$\Delta m/m$	V, 10^{-30} m^{-3}	Calculated $\Delta\theta_p$ (K)	Experiment $\Delta\theta_p$ (K)	Dominant mechanism	References
Rh_2CoSb	Hard magnet	3.6	25%	58	15	15	MCA	This paper
YCo_5	Hard magnet	6.5	4%	17	8		MCA	[9,10]
Fe_2P	Hard magnet	2.5	9%	17	3		MCA	[13]
$Co_3Sn_2S_2$	Hard magnet	0.83	2%	36	2	10	MCA	[31]
Fe_3Sn_2	Frustrated magnet	0.5	2%	27	1	2	MCA	[32,33]
MnBi	Hard magnet	1	5%	49	4		MCA	[11]
MnAs	Easy-plane	−1.2		34	−3	−3	MCA	[34]
Fe_3GeTe_2	2D ferromagnet	1.46	7%	38	4	4	MCA	[15]
CrI_3	2D ferromagnet	0.3	3%	135	3	3	MCA	[16]
$CrGeTe_3$	2D ferromagnet	0.05	1.6%	137	0.5	<1	MCA	[35]
$Fe_{0.25}TaS_2$	2D ferromagnet	3.5		230	58	54	MCA	[36]
Fe	Soft magnet	0.04	0.015%	13	0.04		MCA	[8]
Ni	Soft magnet	−0.005	−0.017%	11	−0.004		MCA	[8]
Gd	Soft magnet	−0.2	−0.07%	33	−0.5	0	MCA	[37]
Tb	Helical (easy plane)	−90		32	−208	−44	MCA and EX	[38]
Dy	Helical (easy plane)	−80		31	−180	−40	MCA and EX	[39]
Ho	Helical (easy plane)	−66		31	−149	−15	MCA and EX	[40]
Er	*c*-axis modulated	10		31	22	29	MCA and EX	[41]
Tm	*c*-axis modulated	30		30	65	58	MCA and EX	[42]
Fe_7S_8	FiM (easy plane)	−2.5		33	−6	−378	MCA and EX	[7]
$CeAgSb_2$	Cycloidal					−63	MCA and EX	[26]
$TbRh_2Si_2$	AFM (easy axis)					120	MCA and EX	[14]

Notes: MCA indicates magnetocrystalline anisotropy; EX indicates exchange; FiM and AFM indicate ferrimagnet and antiferromagnet, respectively. Here, the value of K_1 was used as the room-temperature value for MnBi. This category refers to the magnetic phase just below the magnetic ordering temperature. For heavy rare-earth elements, there are phases with ferromagnetic interactions at low temperatures. Fe_2P, MnBi, and MnAs exhibit first-order transitions at the Curie temperature. Fe_7S_8 has Fe vacancies on every second *ab* plane, and the adjacent plans are antiferromagnetic coupled; therefore, it shows a net magnetic moment and behaves like a ferrimagnet with an in-plane applied magnetic field and an antiferromagnet with an applied out-of-plane field. Both Δm and $\Delta\theta_p$ for cubic Fe and Ni are calculated by the difference from the [001] and [111] directions, whose signs are the same as that of K_1 in cubic systems.

the crystal orientation in materials, such as Rh_2CoSb with such a large anisotropic magnetic performance. Meanwhile, the anisotropic θ_p can be used to estimate the K_1 for some materials that is extremely hard to saturate in the measurement.

V. SUMMARY

Extraordinary anisotropic magnetic properties have been reported for hard magnetic Rh_2CoSb. The magnetization along the *c* axis is 25% larger than that along the *a* axis. Different approaches to the magnetic phase transition are compared and used to describe the transition temperatures, including the critical temperature (to describe the long-range-ordered magnetic structure) and paramagnetic Curie temperatures (to describe the short-range-ordered magnetic structure). The critical temperature and paramagnetic Curie temperatures along the *c* axis are 6 and 15 K higher than those along the *a* axis, respectively, as deduced from the Arrott plots and inverse susceptibility. These values are some of the largest among ferromagnets without an anisotropic exchange. A simple modification of the paramagnetic Curie temperature is performed where the anisotropic value can be estimated from the magnetocrystalline anisotropy rather than from the complicated crystal-field parameters. The modification well explains not only Rh_2CoSb, but also many other previously reported ferromagnetic materials.

ACKNOWLEDGMENTS

This work was financially supported by an Advanced Grant from the European Research Council (Grant No. 742068) "TOPMAT," the European Union's Horizon 2020 Research and Innovation Programme (Grant No. 824123) "SKYTOP," the European Union's Horizon 2020 Research and Innovation Programme (Grant No. 766566) "ASPIN," the Deutsche Forschungsgemeinschaft (Project No. 258499086) "SFB 1143," the Deutsche Forschungsgemeinschaft (Projects No. FE 633/30-1, No. RE 1164/6-1, and No. LU 2261/2-1) "SPP Skyrmionics," the DFG through the Würzburg-Dresden Cluster of Excellence on Complexity and Topology in Quantum Matter ct.qmat (EXC 2147, Project No. 39085490). This work was based on experiments performed at the Swiss Spallation Neutron Source SINQ, Paul Scherrer Institute, Villigen, Switzerland.

[1] Y. He, X. Ke, C. Jiang, N. Miao, H. Wang, J. M. D. Coey, Y. Wang, and H. Xu, Adv. Funct. Mater. **28**, 1800858 (2018).

[2] J. M. D. Coey, *Magnetism and Magnetic Materials* (Cambridge University Press, Cambridge, UK, 2010).

[3] S. Yu. Bodnar, L. Šmejkal, I. Turek, T. Jungwirth, O. Gomonay, J. Sinova, A. A. Sapozhnik, H.-J. Elmers, M. Kläui, and M. Jourdan, Nat. Commun. **9**, 348 (2018).

[4] E. R. Callen and H. B. Callen, J. Phys. Chem. Solids **16**, 310 (1960).

[5] E. R. Callen, J. Appl. Phys. **31**, S149 (1960).

[6] E. R. Callen, Phys. Rev. **124**, 1373 (1961).

[7] J. N. Armstrong, S. Z. Hua, and H. D. Chopra, Phys. Status Solidi B **250**, 387 (2013).

[8] *Handbook of Magnetic Materials*, edited by E. P Wohlfarth (North-Holland, Amsterdam, 1980), Vol. 1.

[9] J. M. Alameda, J. Deportes, D. Givord, R. Lemaire, and Q. Lu, J. Magn. Magn. Mater. **15**, 1257 (1980).

[10] J. M. Alameda, D. Givord, R. Lemaire, and Q. Lu, J. Appl. Phys. **52**, 2079 (1981).

[11] Y. He, S. Schneider, T. Helm, J. Gayles, D. Wolf, I. Soldatov, H. Borrmann, W. Schnelle, R. Schaefer, G. H. Fecher, B. Rellinghaus, and C. Felser, Topological Hall effect arising from the mesoscopic and microscopic non-coplanar magnetic structure in MnBi, arXiv:2011.06340.

[12] M. A. McGuire, H. Cao, B. C. Chakoumakos, and B. C. Sales, Phys. Rev. B **90**, 174425 (2014).

[13] L. Caron, M. Hudl, V. Höglin, N. H. Dung, C. P. Gomez, M. Sahlberg, E. Brück, Y. Andersson, and P. Nordblad, Phys. Rev. B **88**, 094440 (2013).

[14] B. Chevalier, J. Etourneau, J. E. Greedan, J. M. D. Coey, and A. Maaroufi, J. Less-Common. Met. **111**, 171 (1985).

[15] Y. Wang, C. Xian, J. Wang, B. Liu, L. Ling, L. Zhang, L. Cao, Z. Qu, and Y. Xiong, Phys. Rev. B **96**, 134428 (2017).

[16] Y. Liu and C. Petrovic, Phys. Rev. B **97**, 014420 (2018).

[17] P. Boutron, Phys. Rev. B **7**, 3226 (1973).

[18] Y. L. Wang, Phys. Lett. A **35**, 383 (1971).

[19] Y. He, G. H. Fecher, C. Fu *et al.*, Adv. Mater. **32**, 2004331 (2020).

[20] J. Rodríguez-Carvajal, Commission on powder diffraction (IUCr), Newsletter **26**, 12 (2001).

[21] G. H. Fecher, Y. He, and C. Felser, Phys. Rev. Materials **5**, 054404 (2021).

[22] S. K. Dhar, A. K. Grover, S. K. Malik, and R. Vijayaraghavan, Solid State Commun. **33**, 545 (1980).

[23] N. J. Ghimire, M. A. McGuire, D. S. Parker, B. C. Sales, J.-Q. Yan, V. Keppens, M. Koehler, R. M. Latture, and D. Mandrus, Phys. Rev. B **85**, 224405 (2012).

[24] M. K. Chattopadhyay, P. Arora, and S. B. Roy, J. Phys. Condens. Matter. **21**, 296003 (2009).

[25] J. Fan, L. Ling, B. Hong, L. Zhang, L. Pi, and Y. Zhang, Phys. Rev. B **81**, 144426 (2010).

[26] K. D. Myers, S. L. Bud'ko, I. R. Fisher, Z. Islam, H. Kleinke, A. H. Lacerda, and P. C. Canfield, J. Magn. Magn. Mater. **205**, 27 (1999).

[27] M. Szlawska, M. Majewicz, and D. Kaczorowski, J. Alloys Compd. **662**, 208 (2016).

[28] A. V. Andreev, Y. Shiokawa, M. Tomida, Y. Homma, V. Sechovský, N. V. Mushnikov, and T. Goto, J. Phys. Soc. Jpn. **68**, 2426 (1999).

[29] A. Galatanu, Y. Haga, E. Yamamoto, T. D. Matsuda, S. Ikeda, and Y. Ōnuki, J. Phys. Soc. Jpn. **73**, 766 (2004).

[30] Z. Bukowski, V. H. Tran, J. Stepień-Damm, and R. Troć, J. Solid State Chem. **177**, 3934 (2004).

[31] J. Shen, Q. Zeng, S. Zhang, W. Tong, L. Ling, C. Xi, Z. Wang, E. Liu, W. Wang, G. Wu, and B. Shen, Appl. Phys. Lett. **115**, 212403 (2019).

[32] H. Li, B. Ding, J. Chen, Z. Li, Z. Hou, E. Liu, H. Zhang, X. Xi, G. Wu, and W. Wang, Appl. Phys. Lett. **114**, 192408 (2019).

[33] Q. Wang, S. Sun, X. Zhang, F. Pang, and H. Lei, Phys. Rev. B **94**, 075135 (2016).

[34] R. W. De Blois and D. S. Rodbell, Phys. Rev. **130**, 1347 (1963).

[35] S. Selter, G. Bastien, A. U. B. Wolter, S. Aswartham, and B. Büchner, Phys. Rev. B **101**, 014440 (2020).

[36] E. Morosan, H. W. Zandbergen, L. Li, M. Lee, J. G. Checkelsky, M. Heinrich, T. Siegrist, N. P. Ong, and R. J. Cava, Phys. Rev. B **75**, 104401 (2007).

[37] H. E. Nigh, S. Legvold, and F. H. Spedding, Phys. Rev. **132**, 1092 (1963).

[38] D. E. Hegland, S. Legvold, and F. H. Spedding, Phys. Rev. **131**, 158 (1963).

[39] D. R. Behrendt, S. Legvold, and F. H. Spedding, Phys. Rev. **109**, 1544 (1985).

[40] D. L. Strandburg, S. Legvold, and F. H. Spedding, Phys. Rev. **127**, 2046 (1962).

[41] R. W. Green, S. Legvold, and F. H. Spedding, Phys. Rev. **122**, 827 (1961).

[42] D. B. Richards and S. Legvold, Phys. Rev. **186**, 508 (1969).

[43] L. Meng, Z. Zhou, M. Xu, S. Yang, K. Si, L. Liu, X. Wang, H. Jiang, B. Li, P. Qin, P. Zhang, J. Wang, Z. Liu, P. Tang, Y. Ye, W. Zhou, L. Bao, H. Gao, and Y. Gong, Nat. Commun. **12**, 809 (2021).